






## Article

# Harmonic Profile Enhancement of Grid Connected Fuel Cell through Cascaded H-Bridge Multi-Level Inverter and Improved Squirrel Search Optimization Technique

Subhashree Choudhury <sup>1</sup>, Shiba Kumar Acharya <sup>2</sup>, Rajendra Kumar Khadanga <sup>3</sup>, Satyajit Mohanty <sup>4</sup>, Jehangir Arshad <sup>5,\*</sup>, Ateeq Ur Rehman <sup>6</sup>, Muhammad Shafiq <sup>7,\*</sup> and Jin-Ghoo Choi <sup>7,\*</sup>

<sup>1</sup> Department of EEE, Siksha 'O' Anusandhan (Deemed to be University), Bhubaneswar 751030, India; subhashreechoudhury@soa.ac.in

<sup>2</sup> Department of EEE, GITA Autonomous College, Bhubaneswar 752054, India; shibakacharya@gmail.com

<sup>3</sup> Department of EEE, Centurion University of Technology & Management, Bhubaneswar 752050, India; rajendra697@gmail.com

<sup>4</sup> School of Electrical Engineering, Vellore Institute of Technology, Vellore 632014, India; satyajit.mohanty@vit.ac.in

<sup>5</sup> Department of Electrical and Computer Engineering, COMSATS University Islamabad, Lahore 54000, Pakistan

<sup>6</sup> Department of Electrical Engineering, Government College University, Lahore 54000, Pakistan; ateqrehman@gmail.com

<sup>7</sup> Department of Information and Communication Engineering, Yeungnam University, Gyeongsan 38541, Korea

\* Correspondence: jehangirarshad@cuilahore.edu.pk (J.A.); shafiq@ynu.ac.kr (M.S.); jchoi@yu.ac.kr (J.-G.C.)



**Citation:** Choudhury, S.; Acharya, S.K.; Khadanga, R.K.; Mohanty, S.; Arshad, J.; Ur Rehman, A.; Shafiq, M.; Choi, J.-G. Harmonic Profile Enhancement of Grid Connected Fuel Cell through Cascaded H-Bridge Multi-Level Inverter and Improved Squirrel Search Optimization Technique. *Energies* **2021**, *14*, 7947. <https://doi.org/10.3390/en14237947>

Academic Editors: Muhammad Naveed Iqbal and Bilal Asad

Received: 9 November 2021

Accepted: 24 November 2021

Published: 27 November 2021

**Publisher's Note:** MDPI stays neutral with regard to jurisdictional claims in published maps and institutional affiliations.



**Copyright:** © 2021 by the authors. Licensee MDPI, Basel, Switzerland. This article is an open access article distributed under the terms and conditions of the Creative Commons Attribution (CC BY) license (<https://creativecommons.org/licenses/by/4.0/>).

**Abstract:** The generation of energy by conventional systems leads to several environmental issues. Fuel Cell (FC), being a new renewable energy source, has emerged as one of the promising alternatives to obtain clean and efficient energy generation. This paper highlights the power quality enhancement of the grid connected FC through a boost converter and 25 level Cascaded H-Bridge (CHB) Multi-Level Inverter (MLI) using the classical PID controller. To drive the MLI connected to the grid for governing the Point of Common Coupling (PCC) voltage between the FC and the grid, two PID controllers have been utilized. The conventional evolutionary techniques such as Particle Swarm Optimization (PSO) and Squirrel Search Algorithm (SSA) are implemented to tune the PID controllers for dynamic operations. To further enhance the convergence speed of computation and precision of the classical techniques used, an Improved Squirrel Search Algorithm (ISSA) has been proposed in this work. The grid connected power network considered for study here is designed using MATLAB/Simulink environment. Moreover, the system is led to various rigorous voltage sag and swell conditions to test the effectiveness of the proposed controller. A detailed comparison between the conventional PID, PSO, SSA, and proposed ISSA techniques in voltage profile improvement, power quality enhancement, and reduced execution time has been featured. The results obtained highlight the proposed technique's superiority over the classical methods in terms of improved dynamic voltage response, enhanced power quality, and reduced harmonics. The power quality indices are found out using Total Harmonic Distortion (THD) analysis. The values found out are well within the IEEE-547 indices for the proposed controller, thus justifying its real-time implementation.

**Keywords:** Fuel Cell (FC); Solid Oxide Fuel Cell (SOFC); Cascaded H-Bridge (CHB); Particle Swarm Optimization (PSO); Squirrel Search Algorithm (SSA); Improved Squirrel Search Algorithm (ISSA); Oscillatory Transient; voltage sag; voltage swell; Total Harmonic Distortion (THD)

## 1. Introduction

Rising energy demand with improved efficiency and reduced hazardous methods of energy sources are the key aspects of study and research nowadays [1]. The non-renewable energy resources are obsolete due to high cost, less efficiency and not being environmentally

friendly compared to renewable energy sources. Further to lower greenhouse gas emissions, the reduction in fossil fuel is highly required. So for mitigation of the above issues, FC acts as a promising renewable energy source and plays a vital role in delivering clean energy and high efficiency [2].

A fuel cell produces electric current directly from a chemical reaction [3]. Here, the transformation of energy from one form to another is done in one single step for which the losses are less. There are several types of fuel cells like Polymer Electrolyte Membrane Fuel Cell (PEMFC), Direct Methanol, Phosphoric Acid, Molten Carbonate, and Solid Oxide Fuel Cell (SOFC) [4]. This paper uses SOFC as the primary energy source due to its several advantages over other FCs, such as more combined heat, long-term stability, fuel flexibility, and comparatively lower cost. However, the major demerit of SOFC is when employed individually, it cannot compensate the system needs due to its high operating temperature that leads to a longer start time. To eradicate this problem, a PID controller is added to the system [5].

A PID controller is a linear controller that reduces the error but cannot mitigate the non-linearities effectively in the system [6]. For countering this issue, the PID controller parameters value is dynamically tuned by two classical optimization techniques, PSO [7] and SSA [8], already reported in the literature to respond to the system's non-linearity. However, although the PSO and SSA algorithm dynamically responds to change in the system's normal operation, it possesses some disadvantages such as slower convergence speed and precision. So, to counteract the above issues, an ISSA optimization technique has been suggested in this research paper [9].

Furthermore, a 25 level CHB MLI is introduced to enhance the system stability by reducing system harmonics. An MLI gives a low distorted output waveform and limited voltage stress on the switching devices so that the proper sinusoidal waveform of the grid is maintained [10]. In this paper, the proposed ISSA-tuned PID controller is used to enhance MLI switching. The significant advantages of MLI are that it draws current with low distortion, can be operated at both higher and lower frequency, and selective harmonic elimination technique along with the multi-level topology. As a result, the THD becomes low in the output waveform without using any filter circuit [11].

The study proposes the harmonic profile improvement of an SOFC based grid-tied distributed generation system in MATLAB/Simulink architecture. To reduce system oscillations, minimize voltage stress on power electronic interfaces, and maintain the grid output with lesser THD, a 25 level Cascaded H-Bridge inverter has been implemented instead of a conventional two-level inverter. Two PID controllers have been used to drive the MLI interfaced with the grid and govern the Point of Common Coupling (PCC) voltage between the FC and the grid. Furthermore, an ISSA optimization technique has been proposed in this study to dynamically tune the PID controller parameters to respond robustly to any deviation in system operation. The efficacy of the proposed controller has been compared with other conventional techniques through simulation results. It can be concluded from the characteristics obtained that the ISSA method outperforms the traditional SSA and PSO method in achieving better system stability, faster system response, enhanced efficiency, and improved power transfer capability, thus justifying its real-time application. Figure 1 demonstrates the summary of the entire research methodology adopted in the present research work.

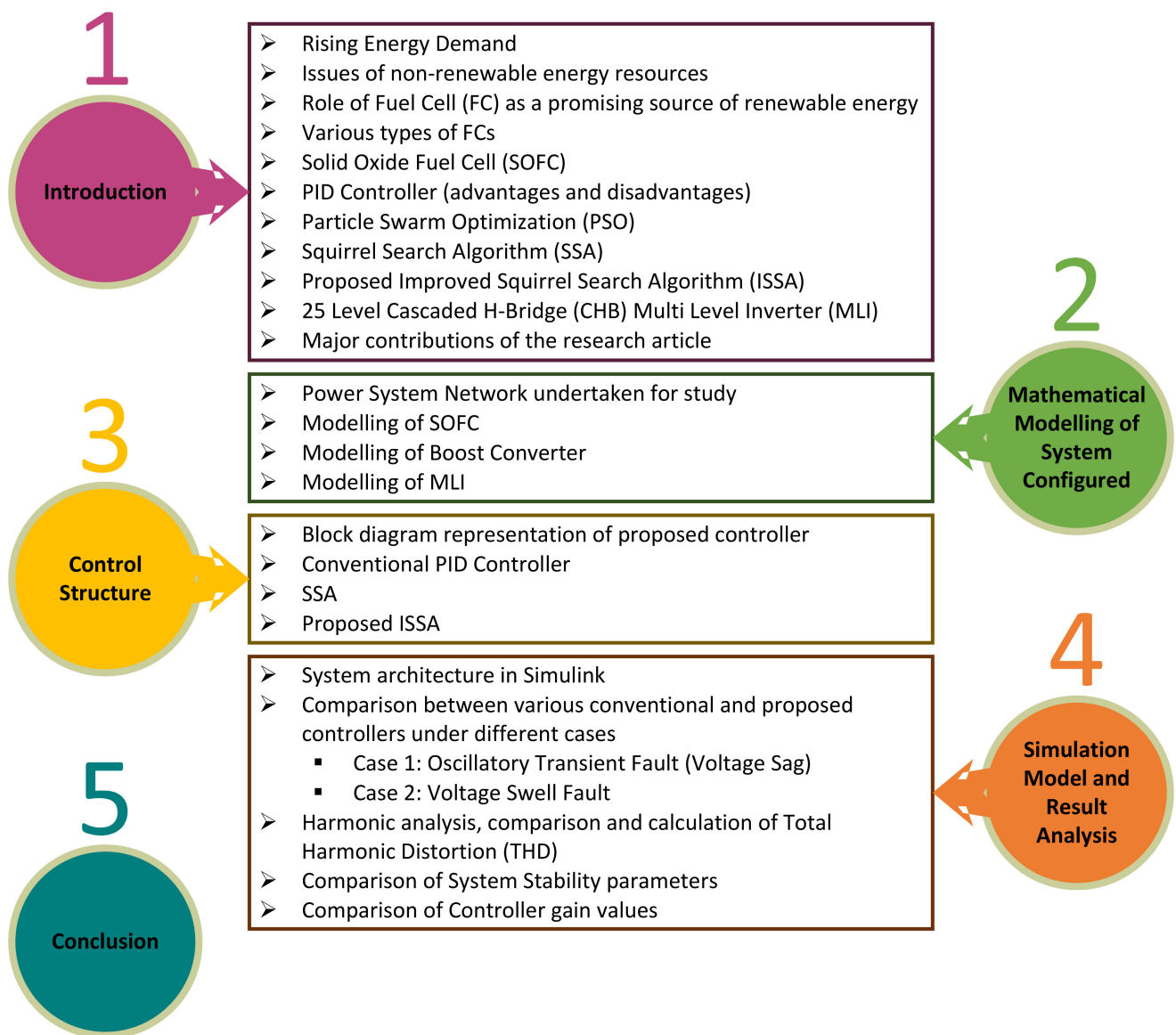


**Figure 1.** Summary of the entire research methodology adopted in the present research work.

The novelty and significant contributions have been highlighted below:

1. Recent evolutionary computational techniques (PSO and SSA) are applied for tuning the PID control parameters for dynamic operation.
2. Design of an improved evolutionary computational technique (ISSA) for faster convergence speed and better precision.
3. The testing of system power quality indices by calculating THD of the conventional and proposed technique.
4. Study of power quality improvement and the dynamic response subjected to swell and sag conditions for the proposed ISSA technique.
5. Use of Solid Oxide Fuel Cell as a distributed generation unit.
6. Two PID controllers are designed to regulate the terminal voltage of the PCC between the SOFC and the power grid by the pulse width modulation (PWM) technique driving the 25 level CHB MLI.

The remaining part of this research work is assembled as follows: In Section 2, the complete system undertaken for the study is detailed with modeling and its related equations. Section 3 presents the structure and the design of the conventional PID controller tuned by classical PSO and SSA techniques and the proposed Improved SSA control technique.

Section 4 illustrates the model designed in MATLAB/Simulink environment, numerical results, and discussions highlighting the effectiveness of the proposed controller over the other classical techniques in optimally and dynamically tuning the PID control parameters to enhance the system's overall transient performance. In Section 5, the conclusion has been given.

## 2. Materials

The power system network considered for the study has been depicted in Figure 2. In addition, the comprehensive modeling of each component of the power system network undertaken has been described in detail below. The detailed values considered for the study have been summarized in Appendix A.

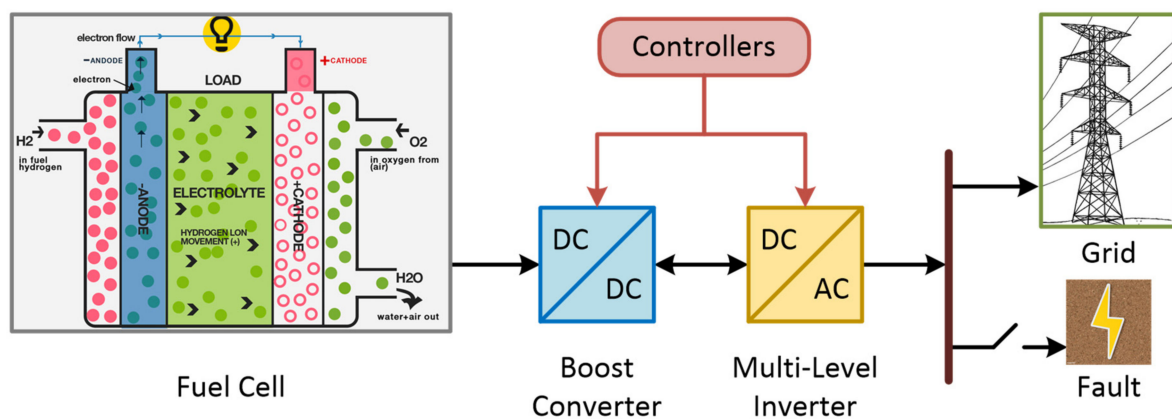


Figure 2. Power system network considered for the study.

### 2.1. SOFC Modelling

A fuel cell is an electrochemical device that converts fuel energy into electrical energy by oxidizing them. A reaction leads this conversion to occur between an oxidant and the fuel [12]. Currently, five types of fuel cells are present, which are as follows: (i) Alkaline (AFC), (ii) Phosphoric Acid (PAFC), (iii) Proton Exchange Membrane (PEMFC), (iv) Molten Carbonate (MCFC) and (v) Solid Oxide (SOFC). Still, SOFC is preferred due to its clean and best technology and high yielding capacity [13]. For effective and safe operation of the SOFC system, the following conditions are necessary: (i) operation at nominal conditions of temperature and pressure, (ii) effective working of all power electronic interfaces with the control units, (iii) proper ambient operation of the thermal and kinetic activities of the feeding system, (iv) a voltage boost system for AC implementation of SOFC is required before converting it to 230 V, 50Hz, AC, (v) electrodes should not contain gas diffused resistances, (vi) right choice of electrolyte to be ensured for proper passage of ions in between the cathode and the anode and (vii) purification of the fuel used by a reformer. A simpler model of a SOFC is designed as depicted in Figure 3 using a voltage source ' $V_0$ ', dependent voltage sources ' $fV_0(I, T)$ ' and ' $V_{act}$ ', capacitor ' $C$ ' and resistors ' $R_a$ ', ' $R_c$ ' and ' $R_0$ '.

The fuel cell voltage at the output end can be formulated as in (1) [12]:

$$U = V - V_1 - V_2 - V_3 \quad (1)$$

where ' $U$ ' is the output end voltage, ' $V$ ' represents the open-circuit voltage, ' $V_1$ ' illustrates the activation voltage across ' $R_a$ ', ' $V_2$ ' denotes the concentration voltage across ' $R_c$ ' and ' $V_3$ ' depicts the drop across the resistor ' $R_0$ '.

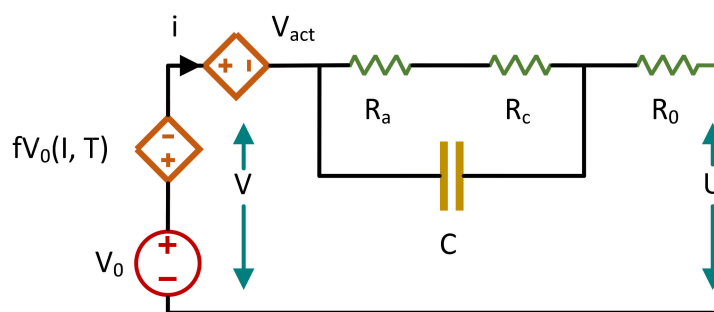


Figure 3. Dynamic model of a SOFC.

Here, the Nernst equation is used to calculate the open-circuit voltage as depicted in (2) [12]:

$$V = N \left[ V_0 + \frac{RT}{2F} \ln \left( \frac{PH_2(P_{O_2})^{0.5}}{PH_2O} \right) \right] \tag{2}$$

where ‘*N*’ depicts the total number of cells, ‘*R*’ represents the universal gas constant (JK/kmol), ‘*T*’ designates the temperature of the cell in Kelvin, ‘*V*<sub>0</sub>’ represents the reversed cell voltage, ‘*PH*<sub>2</sub>’, ‘*P*<sub>O<sub>2</sub></sub>’ and ‘*PH*<sub>2</sub>*O*’ symbolizes the mole fraction value of ‘*H*<sub>2</sub>’, ‘*O*<sub>2</sub>’ and ‘*H*<sub>2</sub>*O*’, respectively.

Activation voltage led by the cell current and the hydrogen moles can be written as in (3) [12]:

$$V_1 = -A * \ln(i) \tag{3}$$

where value ‘*A*’ is decided by the cell type used, and ‘*i*’ is the current flowing through the cell.

Here, concentration voltage can be excluded due to the constant flow of H<sub>2</sub> and O<sub>2</sub> and the operation in the linear region.

The voltage across the resistor ‘*R*<sub>0</sub>’ can be expressed as in (4) [12]:

$$V_3 = i * R_0 \tag{4}$$

### 2.2. Modelling of Boost Converter

It is a DC-DC power converter that steps up the output voltage concerning its input side. It works on a PWM signal that controls the switch’s switching state and leads to different operations inside the converter [14]. Among all DC-DC types of converters, this converter procures a low to medium efficiency range [14]. The basic model of a boost converter can be designed by a voltage source ‘*V*<sub>S</sub>’ as an input, an inductor ‘*L*’, a diode ‘*D*’, a switch ‘*S*’ and a capacitor ‘*C*’ as shown in Figure 4. During the switch-on state, the inductor gets charged and dissipates its energy along with the source voltage, and the switch is turned off to provide an increased voltage at the output end. Thus, the output voltage can be expressed in terms of the input voltage and the duty cycle ‘*T*’ as depicted in (5) [14]:

$$V_0 = \left( \frac{1}{1-T} \right) * V_S \tag{5}$$

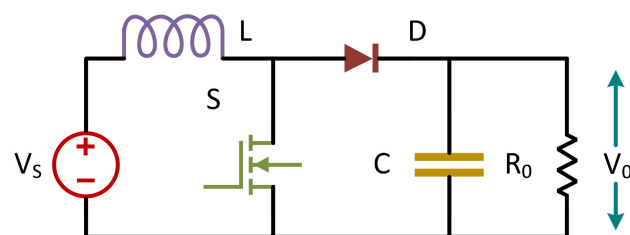


Figure 4. Boost Converter.

### 2.3. Modelling of Multi-Level Inverter (MLI)

An MLI is a power electronic component that uses many low-level DC voltages in the input to provide output alternating voltage as per requirement. It helps to provide a cost-effective solution for managing energy in medium and high voltage power networks [15]. In addition, it possesses many other advantages, such as (1) reducing the THD by making an increase in the voltage waveform; (2) switching frequency for the PWM operation can be reduced, and (3) can generate high voltages by using power electronic components of low rating [16]. Broadly the MLIs can be divided into three types based on switch arrangement and phase angle between them [17,18]: (1) Cascaded H-Bridge (CHB) MLI; (2) Diode Clamped (D-C) MLI, and (3) Flying Capacitor (F-C) MLI. However, the CHB MLI is more promising in comparison to others because (1) it features a high modularity degree; (2) diode or capacitor is not required for clamping; (3) can provide equal voltage level with the use of a reduced number of switches; (4) low losses and stress on the device due to less use of power electronic equipment's and (5) helps to yield better THD. As the CHB based MLI acquires more advantage over others, this paper implements a 25 level CHB MLI to reduce the harmonics and enhance the system's stability under study. Figure 5 represents the 25 levels CHB MLI output voltage waveform of SOFC.

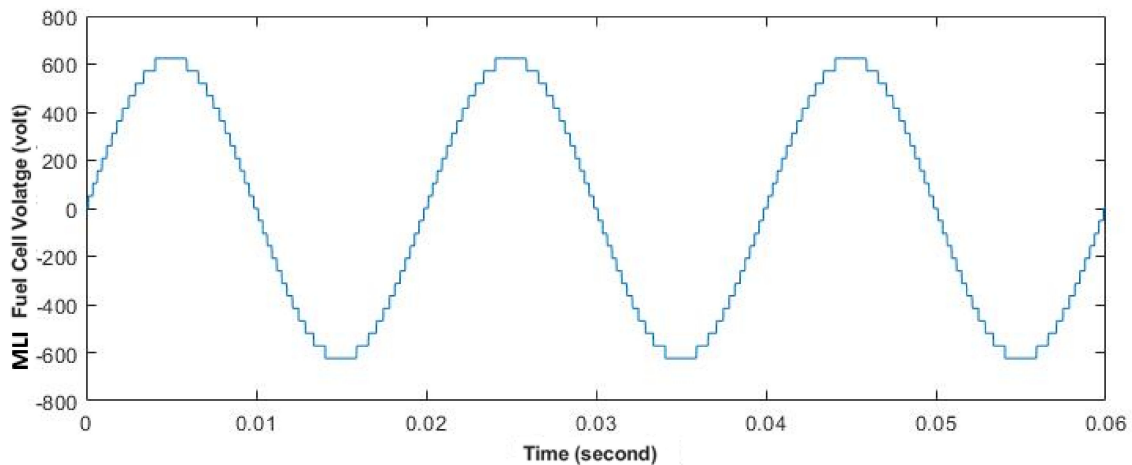


Figure 5. 25 Level Cascaded H-Bridge Multi-Level Inverter Output Voltage waveform of SOFC.

### 3. Methods

Figure 6 depicts the block diagram representation of the proposed controller. The DC output voltage and current of the SOFC are denoted as  $V_{FC}$  and  $I_{FC}$ , respectively. The three-phase output voltage of the inverter at the PCC is represented as  $V_{PCC}$ .  $V_{ref}$  is taken as the reference voltage (assumed to be 1 p.u.) and is compared to the  $V_{PCC}$ . The PID Controller 1 is stimulated by using the error signal  $e_v$  which is the difference in voltages between the reference and PCC. Similarly, the difference in current between the DC output current of the SOFC ( $I_{FC}$ ) and the reference output current at the rated SOFC power ( $I_{ref}$ ) denoted as  $e_i$  is used to stimulate the PID Controller 2. The gate signal of the MLI is derived by the sum of the output of the PID Controller 1 and PID Controller 2 to regulate the PCC voltage at various operating conditions.

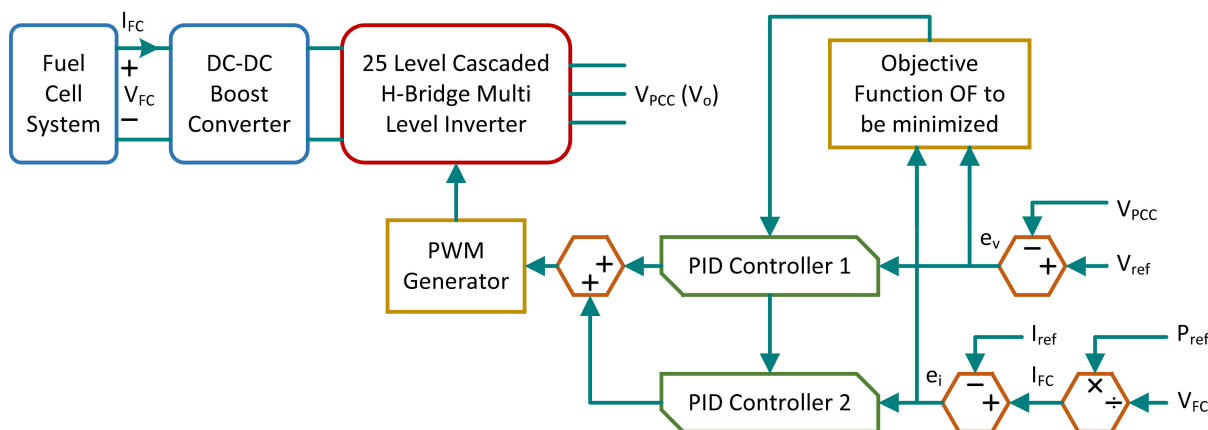


Figure 6. Block Diagram Representation of the proposed controller.

The controller parameters of the two PID Controllers, as shown in Figure 6, are dynamically tuned by the conventional (PSO and SSA) techniques and the proposed ISSA technique to reduce the error signal  $e_v$  with Integral Square Error (ISE) based performance index as given in the equation below for various voltage sag and swell conditions.

The objective function  $OF$  is designed as given in (6):

$$OF = \frac{1}{t} \int_0^t (e_v(t)^2) dt \tag{6}$$

The objective function  $OF$  is a function of the six control parameters of the two PID controllers ( $K_{p1}, K_{i1}, K_{d1}, K_{p2}, K_{i2}$  and  $K_{d2}$ ).

### 3.1. Conventional PID Controller

It is one of the simplest and most linear controllers with three control parameters proportional (P), integration (I), and derivative (D). The three parameters are denoted as  $k_p, k_i$  and  $k_d$  which has decreased the rise time, lowered the steady-state error, and reduced the peak overshoot, thus enhancing the transient response and making the system stable. The parameters of the P, I, and D are dependent on each other [19]. However, the major drawback is that it is linear hence fails to respond dynamically to any change in electrical grid network parameters or non-linearities. The mathematical equation of the PID controller in the time domain and the corresponding transfer function can be represented in (7) and (8), respectively [19].

$$c(t) = k_p e(t) + k_i \int_0^t e(T) + k_d \frac{de(t)}{dt} \tag{7}$$

$$C(s) = k_p + \frac{k_i}{s} + k_d s = \frac{k_d s^2 + k_p s + k_i}{s} \tag{8}$$

### 3.2. Squirrel Search Algorithm (SSA)

SSA is based on the exploring behavior of the southern flying squirrels, discovered in Dry forests of Asia and Europe [20]. The squirrels have an ability well known as ‘gliding’ which they use for their mobility. They change their positions in search of food sources for their daily needs, and the diet they get is from acorn nuts. The presence of predators makes it quite challenging to fulfill their needs, especially in winter because of leaf losses [21]. It makes the squirrels less active in winter. So, they keep searching for an optimal food source that can be stored during winter, such as hickory nuts. After winter is over, the squirrels become more energetic than earlier and again locomote searching for their food.

This life cycle of the squirrels continues throughout their lifetime. The entire process of the SSA is described using a flowchart in Figure 7.

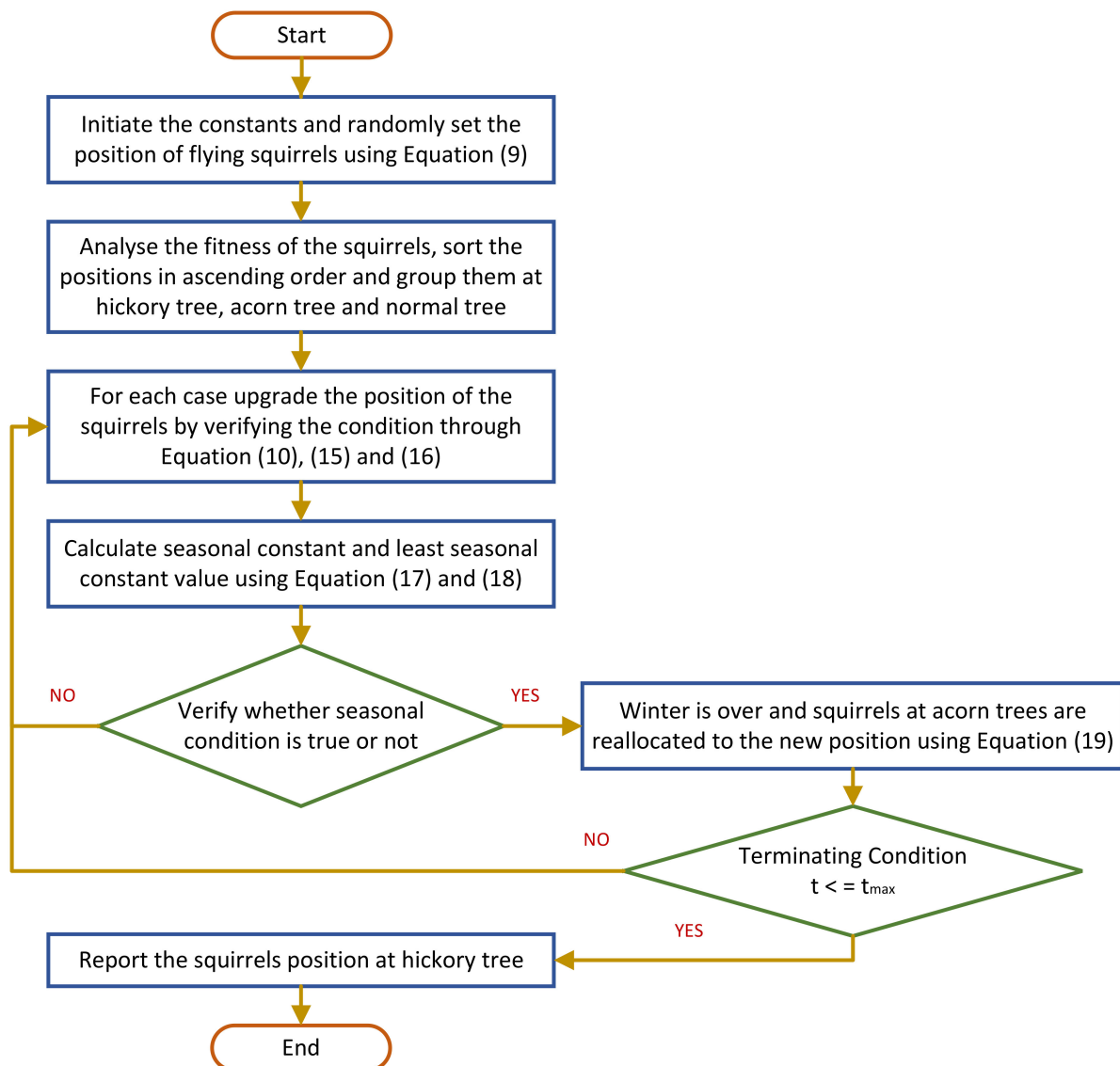


Figure 7. Flowchart of Squirrel Search Algorithm.

Few presumptions are considered for the execution of SSA:

- There is  $x$  number of flying squirrels, and each squirrel is to be present on each tree.
- There are three types of trees: a hickory tree, a normal tree, and an oak tree, in which there is a single hickory tree and a triplet of oak trees.
- All flying squirrels seek food sources and desirably use them [22].

Execution of SSA:

**1. Initiation of Parameters:** Initiating all the constants such as population size ( $x$ ), the maximum number of iteration ( $T$ ), and lower and upper bounds ( $FS_L$  and  $FS_U$ ). Randomly allocating the positions of each flying squirrel according to (9) [20].

$$FS_i = FS_L + rand(1, D) * (FS_U - FS_L) \quad (9)$$

where ' $D$ ' is the dimension of the space,  $i = 1, 2, \dots, x$ .

**2. Fitness Analysis and Grouping:** The position of the flying squirrels is determined by the values calculated through the fitness function [23]. After the positions are arranged



in ascending order, the position of squirrels are grouped into three types: one at the hickory tree ( $FS_{ht}$ ), oak tree ( $FS_{at}$ ) and normal tree ( $FS_{nt}$ ).

### 3. Upgrading of Positions: Three types of cases may occur:

**Case 1-** Flying squirrels on the acorn tree tend to move toward the hickory tree in the absence of predators. So, the new position can be induced using (10) [20].

$$FS_{at}^{t+1} = \begin{cases} FS_{at}^t + d_g * G_c * (FS_{ht}^t - FS_{at}^t), & r1 > P_{dp} \\ \text{Random position,} & \text{otherwise} \end{cases} \quad (10)$$

where ' $G_c$ ' is the gliding constant valued 1.9, ' $r1$ ' is an arbitrary number within the interval [0, 1] and ' $P_{dp}$ ' is predator's existence probability having a constant value of 0.1 and ' $d_g$ ' is the gliding distance which can be calculated using (11) [21].

$$d_g = \frac{h_g}{\tan \varphi * sf} \quad (11)$$

where ' $h_g$ ' is the gliding height having a constant value equals 8, ' $sf$ ' is the scaling factor valued 18, ' $\tan(\varphi)$ ' represents the gliding angle which can be calculated using (12) [21].

$$\tan \varphi = \frac{D}{L} \quad (12)$$

where ' $D$ ' and ' $L$ ' denote the drag force and the lift force severally, which can be calculated using (13) and (14) [22].

$$D = \frac{1}{2\rho V^2 SC_D} \quad (13)$$

$$L = \frac{1}{2\rho V^2 SC_L} \quad (14)$$

where ' $V$ ', ' $S$ ', ' $\rho$ ' and ' $C_D$ ' are constants equal to  $5.25 \text{ ms}^{-1}$ ,  $154 \text{ cm}^2$ ,  $1.204 \text{ kgm}^{-3}$ , and 0.6 severally, and ' $C_L$ ' is a random value within the interval [0.675, 1.5].

**Case 2-** Some flying squirrels on the normal tree tend to move toward acorn trees in the absence of predators. So, the new position can be induced using (15) [22].

$$FS_{nt}^{t+1} = \begin{cases} FS_{nt}^t + d_g * G_c * (FS_{at}^t - FS_{nt}^t), & r2 > P_{dp} \\ \text{Random position,} & \text{otherwise} \end{cases} \quad (15)$$

where ' $r2$ ' is an arbitrary number within the interval [0, 1].

**Case 3-** Considering that the remaining squirrels on the normal tree had fulfilled their food needs. They tend to move toward a hickory tree in the absence of predators. So, the new position can be induced using (16) [21].

$$FS_{nt}^{t+1} = \begin{cases} FS_{nt}^t + d_g * G_c * (FS_{ht}^t - FS_{nt}^t), & r3 > P_{dp} \\ \text{Random position,} & \text{otherwise} \end{cases} \quad (16)$$

where ' $r3$ ' is an arbitrary number within the interval [0, 1].

**4. Testing of Seasonal Condition:** Exploring the behavior of flying squirrels depends on the season. For this, a seasonal constant is calculated through (17) to predict whether winter is over or not and is compared to a minimum seasonal constant value calculated through (18) [20]:

$$S_c = \sqrt{\sum_{k=1}^d (FS_{ai,k} - FS_{hk})^2} \quad (17)$$

$$S_{min} = \frac{10e - 6}{(365)^{t/(T/2.5)}} \quad (18)$$

If condition  $S_c < S_{min}$  is satisfied, winter is over, the squirrels that glided to the hickory tree remain there, and others glided to the acorn tree are reallocated to the new positions [21]. The new positions can be determined by (19) [21].

$$FS_{nt}^{new} = FS_L + levy(n) * (FS_U - FS_L) \quad (19)$$

where 'levy' distribution is used to inflate the ability of optimization and can be calculated from (20) [21].

$$levy(m) = 0.01 * \frac{r_a * \sigma}{|r_b|^{\frac{1}{\beta}}} \quad (20)$$

where ' $\beta$ ' is a constant valued 1.5, ' $\sigma$ ' can be calculated from (21) [21].

$$\sigma = \left( \frac{\Gamma(1 + \beta) * \sin\left(\frac{\pi\beta}{2}\right)}{\Gamma\left(\frac{1+\beta}{2}\right) * \beta * 2^{\left(\frac{\beta-1}{2}\right)}} \right)^{\frac{1}{\beta}} \quad (21)$$

where  $\Gamma(m) = (m - 1)!$

### 3.3. Proposed Improved Squirrel Search Algorithm (ISSA)

ISSA is employed to inflate the ability of the algorithm [24,25], as illustrated in Figure 8. ISSA mainly describe the tactics through which the reliability and speed of the algorithm can be escalated:

**1. Predator's Existence Probability:** The exploring behavior of the flying squirrels are influenced due to the existence of predators and which is governed by  $P_{dp}$ . The populace of flying squirrels is far from their food source, so the range is extensive, thus having a greater chance of being hunted. Throughout the period, they are near their food source, which must reduce their chances of being hunted. So, to adapt this tactic the  $P_{dp}$  is calculated using (22) [25].

$$P_{dp} = (P_{dp\_max} - P_{dp\_min}) * (1 - t/t_{max})^{10} + P_{dp\_min} \quad (22)$$

where ' $P_{dp\_max}$ ' and ' $P_{dp\_min}$ ' are the maximum and minimum probability of the predator's existence, valued at 0.1 and 0.001 severally.

**2. Random Position Induced using Cloud Generator:** Satisfying the condition  $r1, r2, r3 < P_{dp}$ , the squirrels move to a random position, and since they can move to any position and direction due to discrimination in response by each. This can be described by a cloud model, and a new position is induced using a cloud model generator as shown in (23)–(25) [26].

$$FS_{at}^{t+1} = \begin{cases} FS_{at}^t + d_g * G_c * (FS_{ht}^t - FS_{at}^t), & r1 > P_{dp} \\ Cx(FS_{at}^t, En, He), & otherwise \end{cases} \quad (23)$$

$$FS_{nt}^{t+1} = \begin{cases} FS_{nt}^t + d_g * G_c * (FS_{at}^t - FS_{nt}^t), & r2 > P_{dp} \\ Cx(FS_{nt}^t, En, He), & otherwise \end{cases} \quad (24)$$

$$FS_{nt}^{t+1} = \begin{cases} FS_{nt}^t + d_g * G_c * (FS_{ht}^t - FS_{nt}^t), & r3 > P_{dp} \\ Cx(FS_{nt}^t, En, He), & otherwise \end{cases} \quad (25)$$

where ' $He$ ' equals  $0.1 * En$ , and ' $En$ ' is the search radius of the squirrels, which can be known using (26) [26].

$$En = En_{max} * (1 - t/t_{max})^{10} \quad (26)$$

where ' $En_{max}$ ' is the maximum search radius which can be known using (27) [26].

$$En_{max} = (FS_U - FS_L) / 4 \quad (27)$$

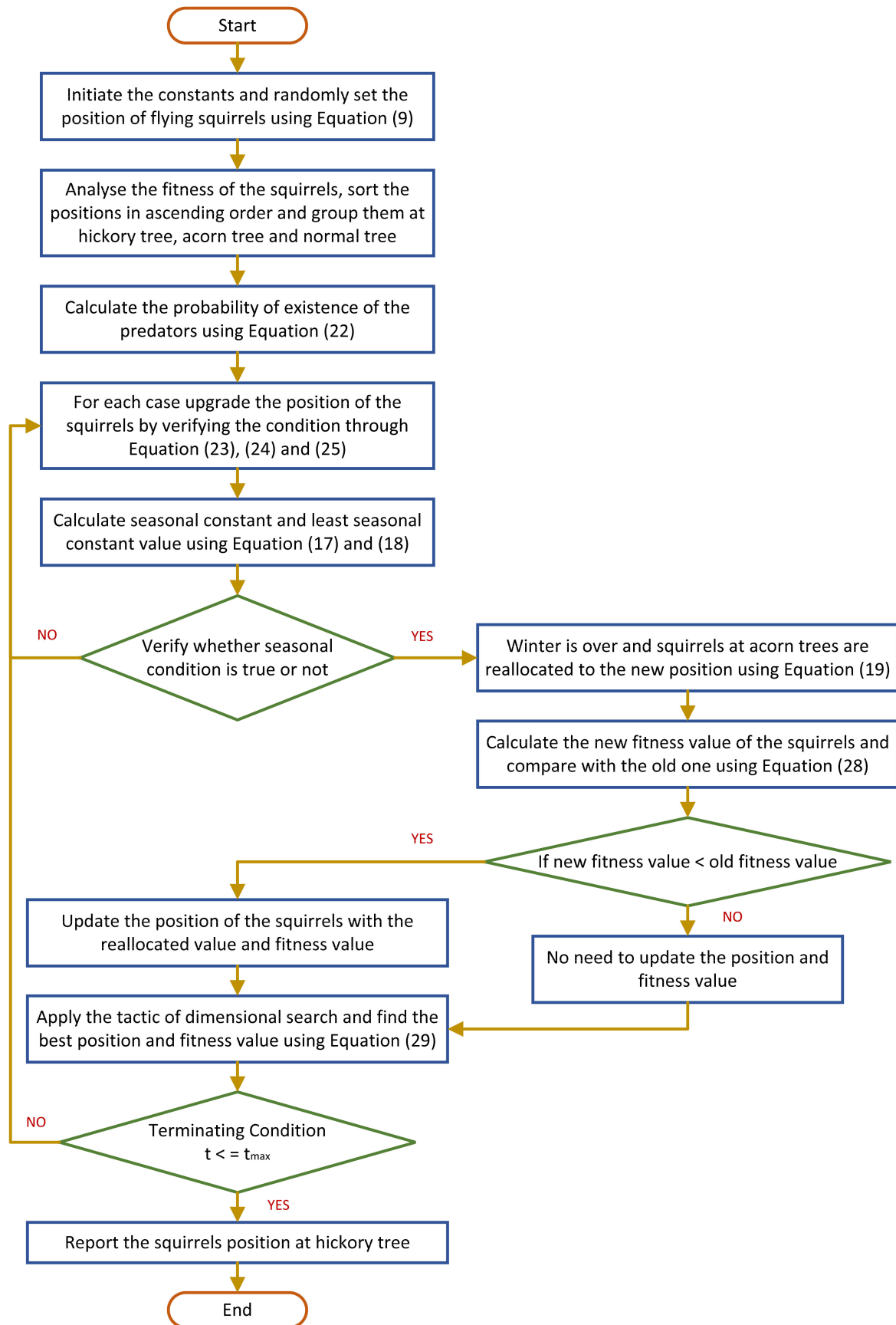


Figure 8. Flowchart of Improved Squirrel Search Algorithm.

**3. Preferring the Best Position:** After the generation of the new position, it may happen that the old position was better. So, in each iteration, it is a must to compare the old fitness value of the squirrels with the new one. If the old fitness value is preferable over the new one, the position of the squirrels will remain unchanged. Otherwise, the new position will be upgraded. It has been explained in (28) [26].

$$FS_i = \begin{cases} FS_i^{new}, & f_i^{new} < f_i^{old} \\ FS_i^{old}, & otherwise \end{cases} \quad (28)$$

**4. Enhancement of Dimensional Search:** In SSA, all dimensions of the flying squirrels are upgraded together. Since the dimensions are dependable and change in one may affect the others, it may prevent them from finding the best solution in their own dimensions [26]. Each iteration is followed by a few steps to inflate the dimensional search.

Discover the best squirrel position. First, induce a similar position by changing one of the dimensional values and the rest keeping the same. Then, compare the fitness value of the original position with the new one and retain the preferable one.

Separately redo steps (ii.) and (iii.) in further dimensions.

The new induced position can be obtained by (29) [26]:

$$FS_{best,j}^{new} = Cx \left( FS_{best,j}^{old}, En, He \right) \quad (29)$$

where  $j = 1, 2, \dots, x$

#### 4. Results and Discussions

This research work proposes an SOFC-based distributed generation system integrated with power electronics equipment like DC-to-DC boost converter and 25 level CHB MLI connected to a three-phase grid in the MATLAB/Simulink environment, as illustrated in Figure 9. To validate and justify the controller action, the system is made prone to two disturbances, such as Oscillatory Transient (Voltage Sag) and Voltage Swell, for time  $t = 0.3$  to  $0.5$  s. Various characteristics of SOFC with the proposed and classical techniques have been studied, compared, and contrasted. Furthermore, the proposed ISSA method is compared with the other SSA- and PSO-based optimization techniques. Further, the effect of reduction in THD has been realized by the MLI in comparison to the conventional two-level inverter.

##### Case 1: Oscillatory Transient Fault (Voltage Sag)

An Oscillatory Transient fault (step decrement of 10%, also known as voltage sag) is applied to the system for time  $t = 0.3$  to  $0.5$  s. The SOFC voltage characteristics for various conventional controllers and proposed controllers have been studied and depicted in Figures 10–14. Figure 10 represents the SOFC voltage during fault time with SOFC-PID, SOFC-PSO-PID, SOFC-SSA-PID, and SOFC-ISSA-PID, respectively. The figures suggest that the proposed ISSA-tuned PID preserves the SOFC voltage at nearly its rated value with enhanced system stability, improved peak time, and rise time compared to the other traditional controllers such as SSA, PSO, and PID.

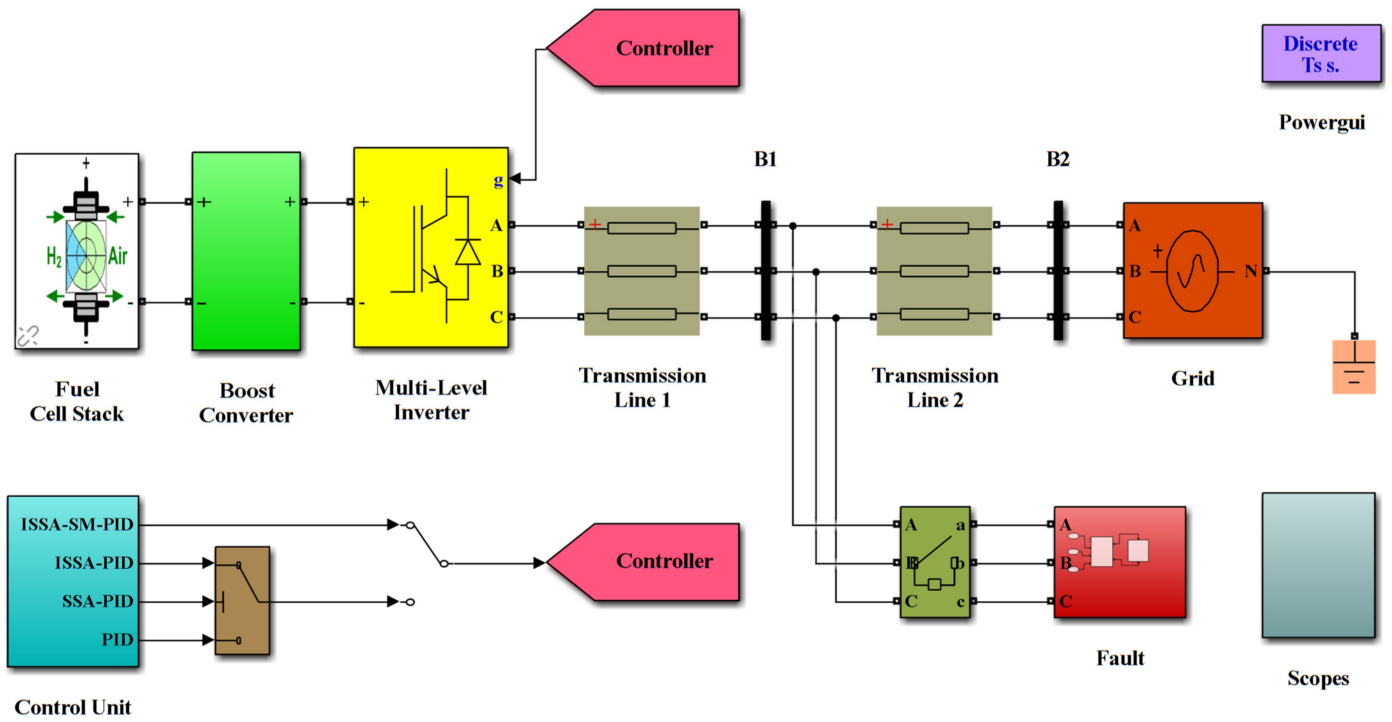


Figure 9. System architecture in Simulink.

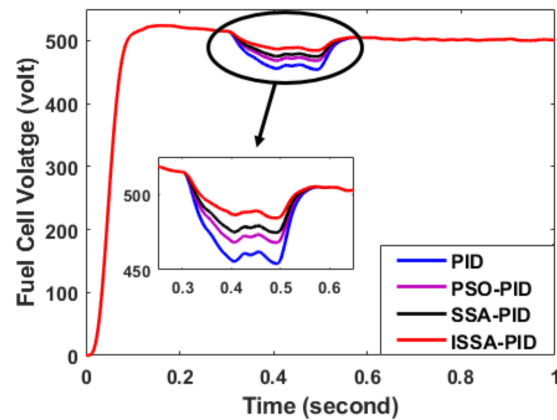


Figure 10. SOFC voltage during fault.

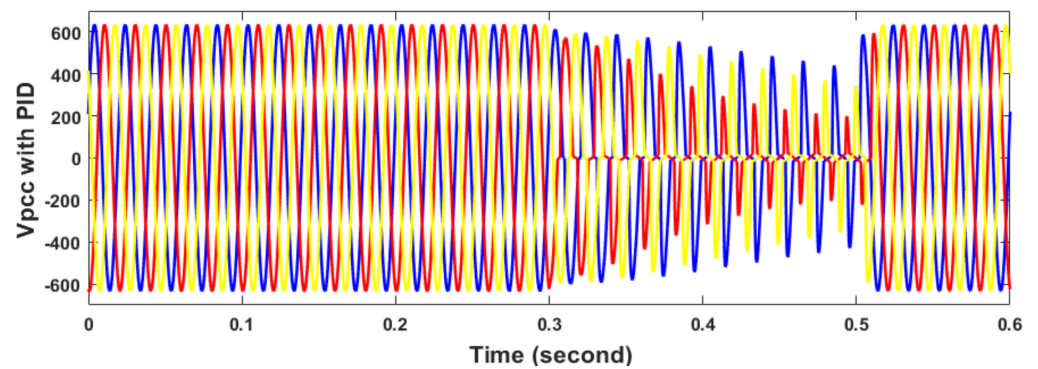


Figure 11. PCC voltage at Fault with PID.

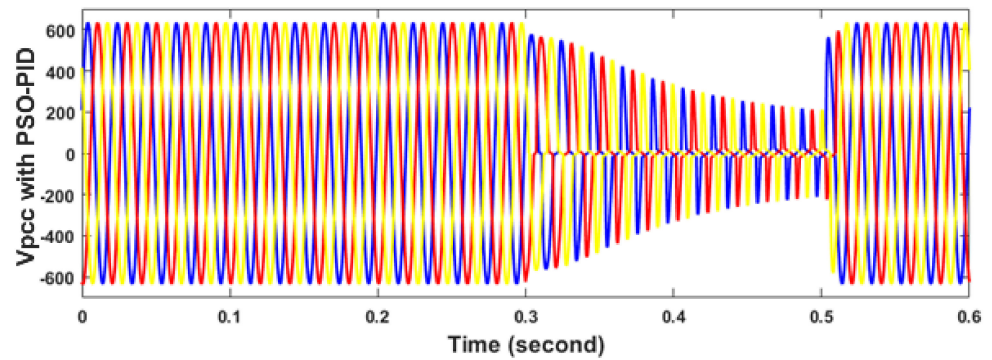


Figure 12. PCC voltage at fault with PSO-tuned PID.

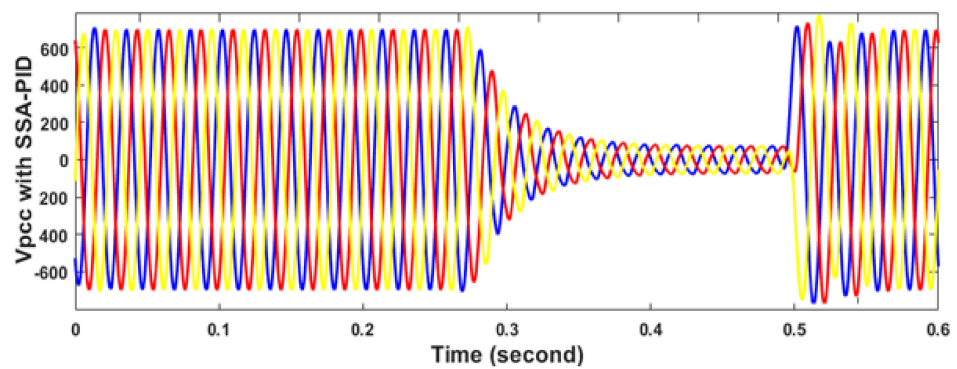


Figure 13. PCC voltage at fault with SSA-tuned PID.

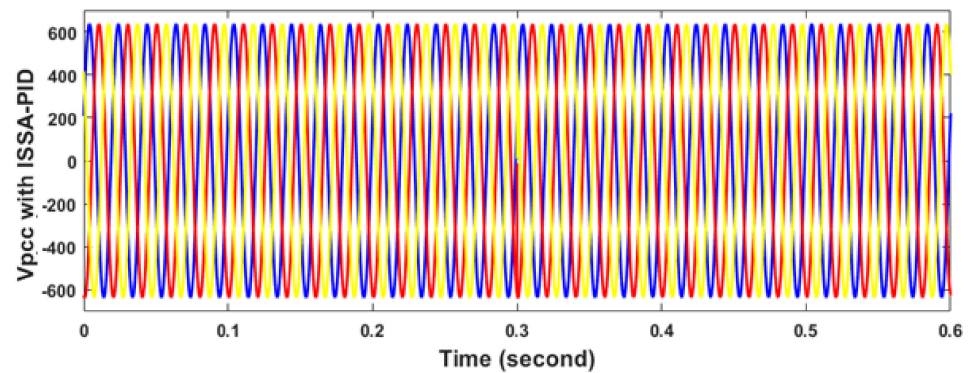


Figure 14. PCC voltage at fault with ISSA-tuned PID.

### Case 2: Voltage Swell Fault

A voltage swell fault (step increase of 10%) is applied to the system for  $t = 0.3$  to  $0.5$  s. Similar to the earlier case, the SOFC voltage and PCC voltage characteristics have been analyzed considering the classical and proposed control methods in Figures 15–19, respectively. The results obtained indicate that the proposed ISSA-tuned PID controller outperforms other techniques in enhancing the maximum spectrum of the voltage of the MLL, introducing best performance in terms of Integral Time Absolute Error (ITAE), enhancing dynamic stability.

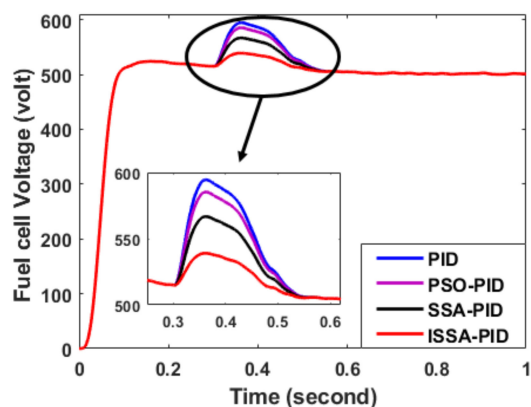


Figure 15. SOFC voltage during Swell Fault.

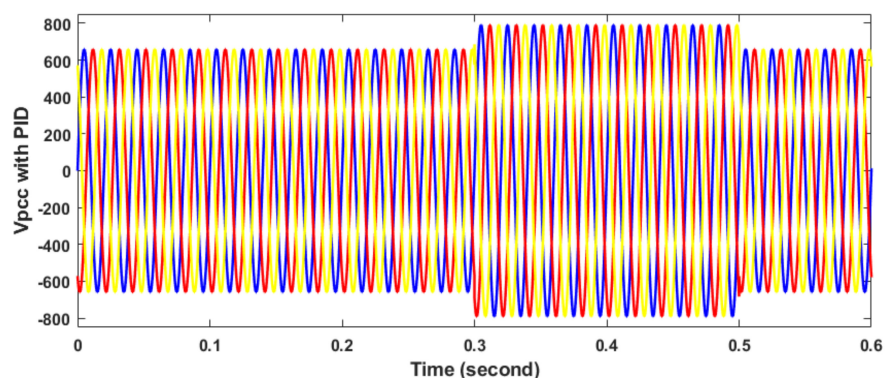


Figure 16. PCC voltage during voltage swell fault with SOFC-PID.

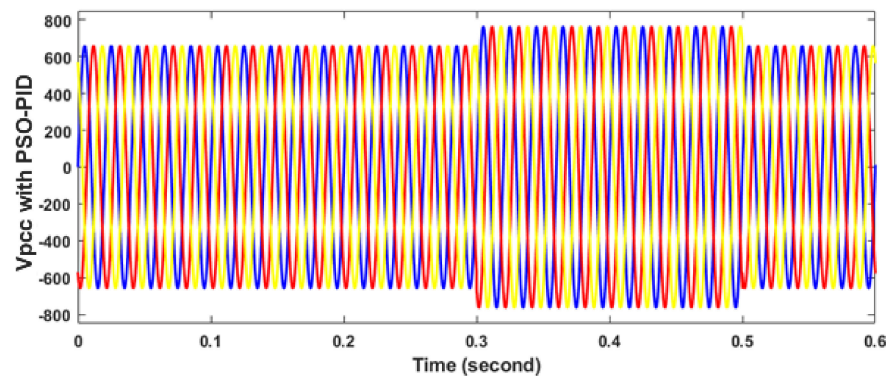


Figure 17. PCC voltage during voltage swell fault with SOFC-PSO-PID.

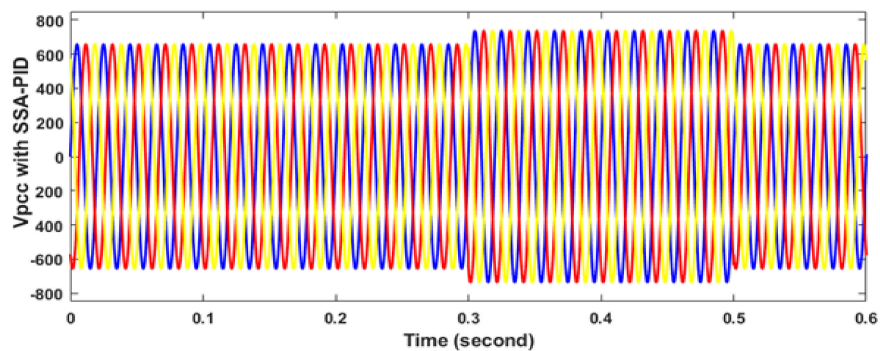


Figure 18. PCC voltage during voltage swell fault with SOFC-SSA-PID.

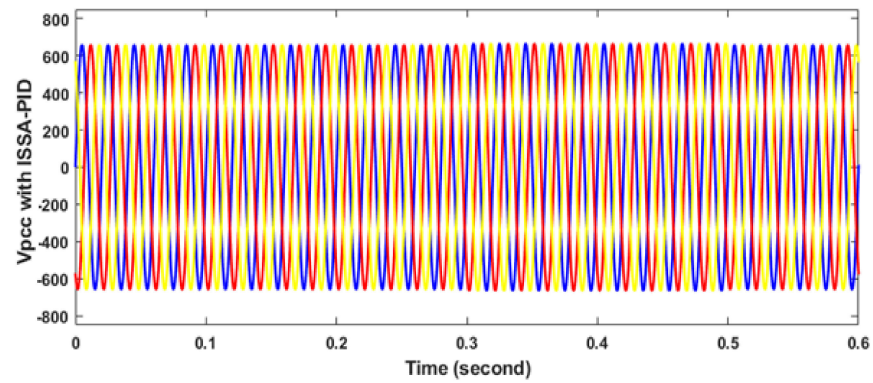


Figure 19. PCC voltage during voltage swell fault with SOFC-ISSA- PID.

Figures 20–23 signify the THD values of the PCC voltage during fault for SOFC-PID, SOFC-PSO-PID, SOFC-SSA-PID, and proposed SOFC-ISSA-PID with MLI, respectively. The computed values of THDs are 0.71%, 1.21%, 4.51, and 5.8%, respectively, which signifies the superiority of the ISSA controller over other controllers in stabilizing the system quicker by mitigating the harmonics present in the system.

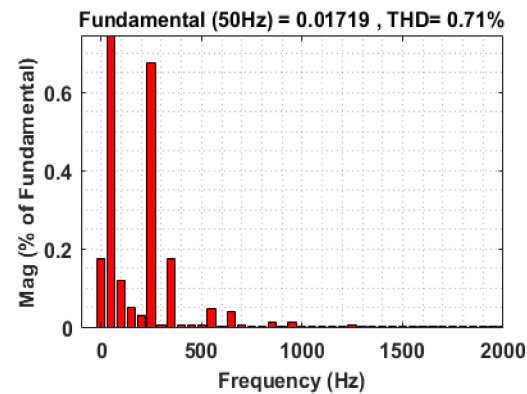


Figure 20. THD of the PCC voltage for ISSA-PID.

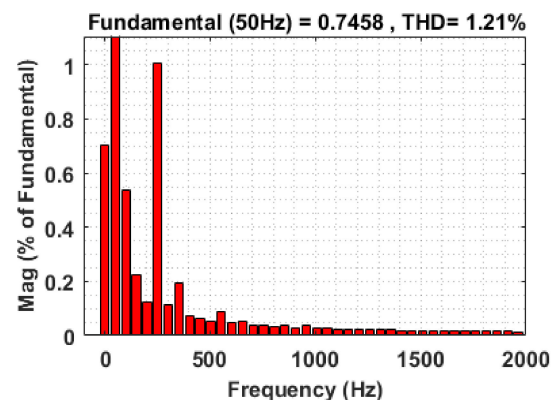


Figure 21. THD of the PCC voltage for SSA-PID.



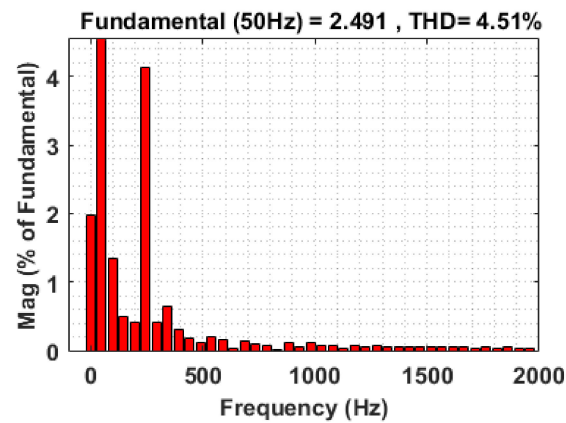


Figure 22. THD of the PCC voltage for PSO-PID.

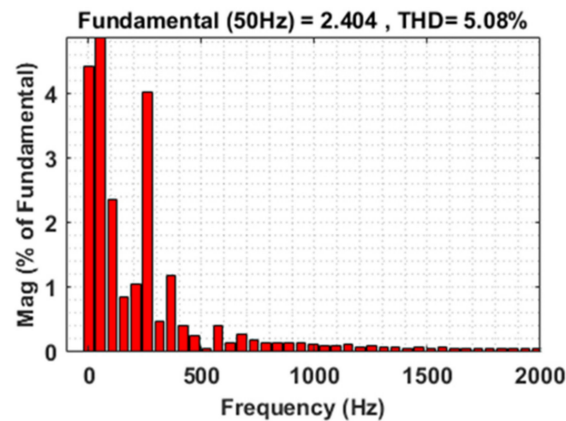


Figure 23. THD of the PCC voltage for PID.

Table 1 summarizes the critical contrast of THD values calculated for SOFC voltage and PCC voltage employing the various controllers and different types of inverters. It can be concluded that the THD values with the proposed technique and the MLI yield the minimum THD value in contrast to other conventional controllers and classical inverter. Table 2 enumerates the statistical comparison of system stability parameters like settling time, peak time, and rise time for various parameters of the microgrid system. From Table 2, it can be inferred that the ISSA-based PID controller has minimum peak time, rise time, and settling time compared to other classical techniques for the SOFC and grid voltage. Table 3 highlights the relative evaluation of controller gain parameters of different types of controllers. It is found that the controller gain values are comparatively lower for the proposed ISSA method compared to SSA- and PSO-based optimization techniques.

**Table 1.** THD Values of the System under Different Controllers.

Cases	Type of Controllers	Types of Inverter			
		Multi-Level Inverter		Classical Inverter	
		Control Parameters			
		$V_{FC}$	$V_{PCC}$	$V_{FC}$	$V_{PCC}$
1	Proposed ISSA Based PID	0.71	0.95	4.51	6.46
	SSA Based PID	1.21	1.52	5.08	7.34
	PSO Based PID	2.23	3.14	6.54	8.41
	Conventional PID	3.81	4.36	9.17	9.25
2	Proposed ISSA Based PID	0.83	1.0	5.82	6.69
	SSA Based PID	1.71	1.88	7.56	7.82
	PSO Based PID	2.79	3.22	8.81	8.99
	Conventional PID	3.96	4.46	9.19	9.80

**Table 2.** System Stability Parameters.

Types of Controller	System Parameters					
	Voltage of FC			Voltage of Grid		
	Peak Time	Rise Time	Settling Time	Peak Time	Rise Time	Settling Time
ISSA-PID	1.53	1.2	1.37	2.13	1.9	1.87
SSA-PID	2.38	2.17	2.28	3.73	2.39	2.91
PSO-PID	3.45	2.93	2.86	4.3	3.7	3.51
PID	5.34	5.23	5.16	7.12	6.117	6.11

**Table 3.** Controller Gain Values.

Controllers → Parameters ↓	ISSA-PID			SSA-PID			PSO-PID			PID		
	$K_p$	$K_i$	$K_d$	$K_p$	$K_i$	$K_d$	$K_p$	$K_i$	$K_d$	$K_p$	$K_i$	$K_d$
FC Voltage	0.2	0.1	0.5	1.1	1.1	1.4	2.1	2.5	2.7	4.5	4.6	4.9
GRID Voltage	0.3	0.1	0.6	1.6	1.9	1.5	2.3	3.9	3.5	5.8	5.8	6.4

## 5. Conclusions

This paper proposes an ISSA optimization technique to enhance power quality and govern the PCC voltage in-between the SOFC and the grid by optimally scheduling the gains of the PID controller used for driving the inverter. The proposed technique is compared with two other conventional optimization techniques, such as PSO and SSA. The system is led to various changes in operating conditions such as voltage sag and swell for justifying the performance of the proposed controller. The characteristics obtained prove that the proposed controller has improved dynamic response during transient conditions and enhanced overshoot compared to other classical methods. The two PID controllers driving the MLI optimized by the proposed ISSA optimization technique enhance the integration of the SOFC with the grid, maintaining the quality of power.

Further, adding a 25 level CHB MLI enhances the system reliability by reducing the harmonics to a greater extent. A detailed comparison between the conventional two-level inverter and MLI considering the THD indices has been made. A comparative analysis of THD values for various optimization techniques has also been presented, and the values obtained are well within the IEEE-517 constraints.

The proposed model and the suggested control method technique can be applied to operate a grid-connected Microgrid system for stability improvement, better system power transfer capability, enhanced efficiency, and achieving output waveforms with reduced harmonics. Furthermore, the simulation results obtained validate that the proposed technique yields improved system control parameters such as improved peak time, rise time, and settling time compared to other methods, thus justifying its application in a global context.

Some of the possible future research works that can be carried out are as follows:

1. The system can be operated with new reduced switch MLIs for better efficiency.
2. Energy storage units can be added to the system undertaken to compensate for the power delivered by the SOFC during extremities.
3. A new optimization technique with a better convergence speed can be implemented.
4. Multiple distributed generation systems such as solar, wind, biomass can be incorporated with SOFC to enhance power delivering capacity.
5. The system can be tested for other faulted conditions for justifying the performance of the proposed controller.

**Author Contributions:** Conceptualization, S.C.; methodology, S.C., J.A., A.U.R., M.S. and J.-G.C.; software, S.C., S.K.A., R.K.K. and S.M.; validation, S.C., J.A., A.U.R., M.S. and J.-G.C.; formal analysis, S.C., S.K.A., R.K.K. and S.M.; investigation, S.C., J.A., A.U.R., M.S. and J.-G.C.; resources, S.C., S.K.A., R.K.K. and S.M.; data curation, S.C., J.A., A.U.R., M.S. and J.-G.C.; writing—original draft preparation, S.C., S.K.A., R.K.K. and S.M.; writing—review and editing, S.C., J.A., A.U.R., M.S. and J.-G.C.; visualization, S.C., S.K.A., R.K.K. and S.M.; supervision, S.C., J.A., A.U.R., M.S. and J.-G.C.; project administration, S.C., S.K.A., R.K.K. and S.M.; funding acquisition, J.-G.C. All authors have read and agreed to the published version of the manuscript.

**Funding:** This work was supported by the MSIT (Ministry of Science and ICT), Korea, under the ITRC (Information Technology Research Center) support program (IITP-2021-2016-0-00313) supervised by the IITP (Institute for Information & Communications Technology Planning & Evaluation).

**Institutional Review Board Statement:** Not applicable.

**Informed Consent Statement:** Not applicable.

**Data Availability Statement:** Authors may provide data on due request.

**Conflicts of Interest:** The authors declare no conflict of interest.

## Abbreviation

FC	Fuel Cell
CHB	Cascaded H-Bridge
MLI	Multi-Level Inverter
PCC	Point of Common Coupling
PSO	Particle Swarm Optimization
SSA	Squirrel Search Algorithm
ISSA	Improved Squirrel Search Algorithm
THD	Total Harmonic Distortion
SOFC	Solid Oxide Fuel Cell
PSO	Particle Swarm Optimization
PEMFC	Polymer Electrolyte Membrane Fuel Cell
PWM	Pulse Width Modulation
AFC	Alkaline Fuel Cell
PAFC	Phosphoric Acid Fuel Cell
PEMFC	Proton Exchange Membrane Fuel Cell
MCFC	Molten Carbonate Fuel Cell
D-C	Diode Clamped
F-C	Flying Capacitor
ISE	Integral Square Error
ITAE	Integral Time Absolute Error

## Appendix A

**Table A1.** System component specifications.

System Components	Values
FC	$V_0 = 60$ , $R_1 + R_2 = 1.4 \Omega$ , $R_3 = 1.06$ , $C = 1.25 \text{ F}$
Boost	$L = 0.5 \text{ mH}$ , $C = 100 \mu\text{F}$ , $F_s = 20 \text{ KHz}$ , $V_0 = 500$ , $V_{in} = 60 \text{ V}$
MLI	IGBTs = 14, Gate Driver Circuit = 11 $V_{OUT} = 500 \text{ V}$
Transmission Line Parameters	Resistance = $0.01755 \Omega$ , Inductance = $0.8737 \times 10^{-3} \text{ H}$ , Capacitance = $13.33 \times 10^{-9} \text{ F}$
Grid	$V = 600$ , $X/R = 9$ , $F = 50 \text{ Hz}$
Fault type	Values
Oscillatory Transient	Capacitance = $2000 \times 10^{-6} \text{ F}$ , $F = 40 \text{ HZ}$
Swell	Resistive Load = $1000 \Omega$ , Capacitance = $2500 \times 10^{-6} \text{ F}$ , Inductance = $5 \times 10^{-3} \text{ H}$

## References

- Mottaghizadeh, P.; Fardadi, M.; Jabbari, F.; Brouwer, J. Thermal Management of Dynamic Operation of Solid Oxide Cell-Based Energy Storage System for 2 Renewable Electricity Scenarios. *ECS Meet. Abstr.* **2019**, 2187. [\[CrossRef\]](#)
- Akinyele, D.; Olabode, E.; Amole, A. Review of Fuel Cell Technologies and Applications for Sustainable Microgrid Systems. *Inventions* **2020**, *5*, 42. [\[CrossRef\]](#)
- Shabri, H.A.; Othman, M.H.D.; Mohamed, M.A.; Kurniawan, T.A.; Jamil, S.M. Recent progress in metal-ceramic anode of solid oxide fuel cell for direct hydrocarbon fuel utilization: A review. *Fuel Process. Technol.* **2021**, *212*, 106626. [\[CrossRef\]](#)
- Sazali, N.; Salleh, W.N.W.; Jamaludin, A.S.; Razali, M.N.M. New Perspectives on Fuel Cell Technology: A Brief Review. *Membranes* **2020**, *10*, 99. [\[CrossRef\]](#)
- Bansal, H.O.; Sharma, R.; Shreeraman, P.R. PID controller tuning techniques: A review. *J. Control. Eng. Technol.* **2012**, *2*, 168–176.
- Chopra, V.; Singla, S.K.; Dewan, L. Comparative analysis of tuning a PID controller using intelligent methods. *ACTA Polytech. Hung.* **2014**, *11*, 235–249.
- Solihin, M.I.; Tack, L.F.; Kean, M.L. Tuning of PID controller using particle swarm optimization (PSO). In Proceedings of the International Conference on Advanced Science, Engineering and Information Technology, Bangi-Putrajaya, Malaysia, 14–15 January 2011.
- Fares, D.; Fathi, M.; Shams, I.; Mekhilef, S. A novel global MPPT technique based on squirrel search algorithm for PV module under partial shading conditions. *Energy Convers. Manag.* **2021**, *230*, 113773. [\[CrossRef\]](#)
- Zheng, T.; Luo, W. An Improved Squirrel Search Algorithm for Optimization. *Complexity* **2019**, *2019*, 6291968. [\[CrossRef\]](#)
- Choudhury, S.; Bajaj, M.; Dash, T.; Kamel, S.; Jurado, F. Multi-level Inverter: A Survey on Classical and Advanced Topologies, Control Schemes, Applications to Power System and Future Prospects. *Energies* **2021**, *14*, 5773. [\[CrossRef\]](#)
- Ray, S.; Gupta, N.; Gupta, R.A. Power quality improvement using multi-level inverter-based active filter for medium-voltage high-power distribution system: A comprehensive review. *Int. J. Power Electron.* **2021**, *14*, 1–36. [\[CrossRef\]](#)
- Choudhury, S.; Sen, B.; Kumar, S.; Sahani, S.; Pattnaik, A.; Dash, T. Improvement of Performance and Quality of Power in Grid Tied SOFC through Crow Search Optimization Technique. In Proceedings of the 2020 5th International Conference on Communication and Electronics Systems (ICCES), Coimbatore, India, 10–12 June 2020; pp. 68–73.
- Damo, U.M.; Ferrari, M.; Turan, A.; Massardo, A. Solid oxide fuel cell hybrid system: A detailed review of an environmentally clean and efficient source of energy. *Energy* **2019**, *168*, 235–246. [\[CrossRef\]](#)
- Hu, X.; Ma, P.; Wang, J.; Tan, G. A Hybrid Cascaded DC–DC Boost Converter with Ripple Reduction and Large Conversion Ratio. *IEEE J. Emerg. Sel. Top. Power Electron.* **2020**, *8*, 761–770. [\[CrossRef\]](#)
- Mondol, M.H.; Tür, M.R.; Biswas, S.P.; Hosain, M.K.; Shuvo, S.; Hossain, E. Compact three phase multi-level inverter for low and medium power photovoltaic systems. *IEEE Access* **2020**, *8*, 60824–60837. [\[CrossRef\]](#)
- Pawar, N.; Tayal, V.K.; Choudekar, P. Design of Cascaded H-Bridge Multilevel Inverter. In *Advances in Smart Communication and Imaging Systems. Lecture Notes in Electrical Engineering*; Agrawal, R., Kishore, S.C., Goyal, A., Eds.; Springer: Singapore, 2021; Volume 721, pp. 645–655. [\[CrossRef\]](#)
- Abd Halim, W.; Ganeson, S.; Azri, M.; Azam, T.T. Review of multi-level inverter topologies and its applications. *J. Telecommun. Electron. Comput. Eng.* **2016**, *8*, 51–56.
- Siahbalaee, J.; Sanaie, N. Comparison of conventional and new cascaded multi-level inverter topologies based on novel indices. *ISA Trans.* **2022**, *119*, 41–51. [\[CrossRef\]](#)
- Khodabakhshian, A.; Hooshmand, R. A new PID controller design for automatic generation control of hydro power systems. *Int. J. Electr. Power Energy Syst.* **2010**, *32*, 375–382. [\[CrossRef\]](#)

20. Choudhury, S.; Khandelwal, N. A Novel Weighted Superposition Attraction Algorithm-based Optimization Approach for State of Charge and Power Management of an Islanded System with Battery and SuperCapacitor-based Hybrid Energy Storage System. *IETE J. Res.* **2020**, 1–14. [[CrossRef](#)]
21. Ponnuvel, S.V.; Murugesan, S.; Duraisamy, S.P. Multi-objective squirrel search algorithm to solve economic environmental power dispatch problems. *Int. Trans. Electr. Energy Syst.* **2020**, *30*, e12635. [[CrossRef](#)]
22. Jain, M.; Singh, V.; Rani, A. A novel nature-inspired algorithm for optimization: Squirrel search algorithm. *Swarm Evol. Comput.* **2019**, *44*, 148–175. [[CrossRef](#)]
23. Sakthivel, V.P.; Suman, M.; Sathya, P.D. Combined economic and emission power dispatch problems through multi-objective squirrel search algorithm. *Appl. Soft Comput.* **2021**, *100*, 106950. [[CrossRef](#)]
24. Wang, Y.; Du, T. An Improved Squirrel Search Algorithm for Global Function Optimization. *Algorithms* **2019**, *12*, 80. [[CrossRef](#)]
25. El-Ashmawi, W.H.; Elminaam, D.S.A. A modified squirrel search algorithm based on improved best fit heuristic and operator strategy for bin packing problem. *Appl. Soft Comput.* **2019**, *82*, 105565. [[CrossRef](#)]
26. Zhang, X.; Zhao, K.; Wang, L.; Wang, Y.; Niu, Y. An Improved Squirrel Search Algorithm With Reproductive Behavior. *IEEE Access* **2020**, *8*, 101118–101132. [[CrossRef](#)]